



Effect of hydrogen spillover in selective hydrodesulfurization of FCC gasoline over the CoMo catalyst



Bin Liu^a, Lei Liu^a, Zhong Wang^b, Yongming Chai^a, Huan Liu^a, Changlong Yin^a, Chenguang Liu^{a,*}

^a State Key Laboratory of Heavy Oil Processing, Key Laboratory of Catalysis of China National Petroleum Corporation (CNPC), China University of Petroleum (East China), Qingdao 266555, PR China

^b Fushun Petrochemical Company, PetroChina, Fushun 113001, PR China

ARTICLE INFO

Article history:

Received 20 February 2016

Received in revised form 3 August 2016

Accepted 11 August 2016

Available online 3 September 2016

Keywords:

Hydrodesulfurization

Synergism

Spillover hydrogen

Selectivity

ABSTRACT

The synergism of promoter Co on the performance of MoS₂ phase in selective hydrodesulfurization (HDS) of FCC gasoline was studied by regulating the step impregnation-sulfurization sequence of Co and Mo species to adjust the proportion of Co-Mo-S phase, separated Co₉S₈ and MoS₂ phases. The evaluation results demonstrated that the CoMo/γ-Al₂O₃ catalyst with Co species first impregnation-sulfurization showed higher HDS activity and selectivity. The characterization by XRD, HRTEM, XPS, TPR and FT-IR showed that, on this catalyst, the interaction between the sulfurized Co and MoS₂ phases was weak, and lead to the lower Co decoration on the MoS₂ phase, thus forming more Co₉S₈ phase. **The more formed Co₉S₈ phase could produce more hydrogen spillover (Hso) to create more CUS and SH groups, thus greatly improving the HDS activity and selectivity.** Through the layered loading test of Co₉S₈/γ-Al₂O₃ and MoS₂/γ-Al₂O₃ catalysts, it was found that the Hso synergistic effect between the Co₉S₈ and MoS₂ phases could significantly improve the HDS activity, but showed very little effect on the saturation of olefins.

© 2016 Published by Elsevier B.V.

1. Introduction

People's growing environmental protection awareness and stringently promulgated legislation to control the exhaust gas (SO_x and NO_x) emission from motor vehicles promote the continuous improvements in ultraclean gasoline production. In addition to major sulfur content, FCC gasoline also contains massive olefins which are important to maintain the high octane number of the final product. However, octane-boosting olefins could be easily hydrogenated during the hydrodesulfurization (HDS) reaction [1]. It was widely accepted that the final morphology of the (Co)MoS₂ active phase is closely related to its catalytic properties [2]. Therefore, in-depth understanding of that could provide a theoretical basis for the tailored preparation of catalysts with optimal activity and selectivity.

Many efforts are continuously focused on the study of structure–activity/selectivity relationship in HDS process. No uniform conclusion on the synergistic effect of cobalt as promoter is obtained. The synergism between Co and Mo has been mainly

explained by two typical active phase models: the Co-Mo-S phase model and the remote control model [3–5]. The Co-Mo-S phase model proposed firstly by Topsøe et al. [6–9] was consisted of highly dispersed MoS₂ nanocrystallites decorated with the Co atoms located at the edge and corner sites, the CoAl₂O₄ and Co₉S₈ species. The Co₉S₈ species was considered to be inactive and even detrimental to the catalytic activity. Many experimental results and advances in hydrotreating catalysis could be explained by the Co-Mo-S model [10]. However, a large number of previous studies also found that the mechanical mixtures of the Co₉S₈ and the MoS₂ crystallites showed much higher catalytic activity than that of the sum of the separated Co₉S₈ and MoS₂ particle. It could be explained by the remote control model [11], in which hydrogen spillover (Hso) migrate from a donor to an acceptor phase and thus influence the HDS activity of the acceptor. Moreover, for the unsupported Co-Mo catalysts, Prins et al. [12] found that the Co ions firstly located at the edge and corner sites of the MoS₂ crystallites to form the Co-Mo-S phase while the Co content was low, greatly promoted the HDS reaction. In addition, the Co₉S₈ phase was also found as a support or carrier with high Co content, which could further improve the HDS activity. The synergism between probably Co₉S₈ and MoS₂ particles had been confirmed by using stacked beds experiment, composed of a donor bed Co/SiO₂ to form Hso, a separator bed SiO₂

* Corresponding author.

E-mail address: cgliu@upc.edu.cn (C. Liu).

to transfer H_{so} and an acceptor bed Mo/SiO₂ to accept H_{so}. Under these conditions, the formation of the Co-Mo-S phase was completely impossible, the synergism was consequently attributed to the H_{so} proposed by the remote control model [11]. Meanwhile, the synergism was widely existed between other metal sulfides (Mn, Fe, Cu, Zn, Ru) and the MoS₂ particles [13]. Using γ-Al₂O₃ or SiC instead of SiO₂ as the separator could also confirmed the synergism effect [14–16]. The distance between the donor and acceptor in stacked beds is much longer than the distance in real catalysts (less than 1 nm). Therefore, it was reasonably estimated that the spillover might be much more efficient in real catalysts.

The synergism effect produced by spillover could affect the HDS reaction path, thus affecting the HDS activity and selectivity. It was found that the contribution of the HYD reaction of DBT to cyclohexylbenzene was higher than that of the direct desulfurization pathway from DBT to biphenyl in the stacked bed reactor [17–20]. However, the direct desulfurization route is strongly enhanced by the presence of Co in a sulfurized CoMo/γ-Al₂O₃ catalyst, while the hydrogenation reaction is hardly enhanced [21]. Most research of spillover hydrogen usually focus on the selectivity and activity of S-compounds' desulfurization normally using gas oil and model feedstocks, such as DBT and 4,6-DMDBT. The olefins, which are important to maintain the high octane number of the final product could be easily saturated in the HDS reaction [22]. To our knowledge, few researchers have investigated the hydrogen spillover effect in selective HDS of FCC gasoline, especially the hydrogen spillover effect in hydrogenation (HYD) of olefins.

Therefore, the aim of the work was to illuminate the synergism between Co and Mo through regulating the impregnation sequence of the active components Co and Mo to adjust the formation probability of Co-Mo-S phase and the separated Co₉S₈ and MoS₂ phase. Moreover, the effect of H_{so} in selective HDS of FCC gasoline, especially the hydrogen spillover effect in olefin HYD reaction was first studied by using a single bed and stacked beds catalyst system.

2. Experimental

2.1. Catalysts preparation

2.1.1. Unsupported catalysts preparation

The unsupported MoS₂ and Co₉S₈ catalysts were prepared from (NH₄)₂MoS₄ (ATTM) and Co(NO₃)₂·6H₂O by sulfiding in a mixture of 10 vol.% H₂S/H₂ at 400 °C for 3 h, respectively. The unsupported Co₉S₈-MoS₂ catalyst was prepared by impregnating the unsupported Co₉S₈ catalyst with ATTm solution followed by drying at 60 °C for 12 h and sulfiding in 10 vol.% H₂S/H₂ at 400 °C for 3 h. The unsupported MoS₂-Co₉S₈ catalyst was prepared by impregnating the unsupported MoS₂ catalyst with cobalt nitrate followed by drying at 60 °C for 12 h and sulfiding in 10 vol.% H₂S/H₂ at 400 °C for 3 h. The Co₉S₈/MoS₂ catalyst was prepared by mechanical mixing of unsupported MoS₂ and Co₉S₈ catalyst.

2.1.2. Supported catalysts preparation

The trifolium γ-Al₂O₃ extrudates were prepared in the laboratory with an external diameter of 1.2 mm, an average length of 2 mm, a BET surface area of 269 m² g⁻¹, pore volume of 0.74 cm³ g⁻¹ and a BJH average pore diameter of 7.2 nm. The MoS₂/γ-Al₂O₃ catalyst was prepared by incipient wetness impregnation of γ-Al₂O₃ with a solution of ATTm, followed by dried at 60 °C for 3 h in air and calcined at 400 °C for 3 h in a 10 vol.% H₂S/H₂ atmosphere. The Co₉S₈/γ-Al₂O₃ catalyst was prepared by incipient wetness impregnation of γ-Al₂O₃ with an aqueous solution of Co(NO₃)₂·6H₂O, followed by calcined at 500 °C for 3 h in air and sulfided at 400 °C for 3 h in 10 vol.% H₂S/H₂ atmosphere.

The CoMo-supported catalysts were prepared by step impregnation method with two different sequences. The MoS₂ + Co₉S₈/γ-Al₂O₃ catalyst was prepared by incipient wetness impregnation of the MoS₂/γ-Al₂O₃ catalyst with an aqueous solution of Co(NO₃)₂·6H₂O, and then sulfided at 400 °C for 3 h in 10 vol.% H₂S/H₂ atmosphere. The Co₉S₈ + MoS₂/γ-Al₂O₃ catalyst was prepared by incipient wetness impregnation of the Co₉S₈/γ-Al₂O₃ catalyst with an aqueous solution of ATTm, and then sulfided at 400 °C for 3 h in 10 vol.% H₂S/H₂ atmosphere. The concentrations of all catalysts compositions were similar, 9.3 wt.% of MoO₃ and/or 2.7 wt.% of CoO obtained by X-ray fluorescence (XRF) analysis.

2.2. Characterization of catalysts

A detailed description of all characterization techniques have been provided elsewhere [23], and only a brief summary was given here. X-ray powder diffraction (XRD) patterns of the catalysts were obtained with a PANalytical's X'Pert PRO diffractometer by using Cu-Kα radiation operated at 45 kV and 40 mA with the scan rate of 8°/min and 2θ range of 5–75°. Temperature-programmed reduction (TPR) was performed on a Quantachrome ChemBET 3000 instrument. In order to remove the adsorbed materials, the sample was pretreated at 150 °C for 1 h under He flow. The sample was reduced in 10 vol.% H₂/Ar (100 ml/min) at a heating rate of 10 °C/min to 800 °C. The consumption of hydrogen was detected through a thermal conductivity detector (TCD). The HRTEM images of the samples were taken using a JEOL JEM-2100 FX microscope. The catalysts were firstly etched by hydrofluoric acid and then suspended in alcohol by an ultrasonic bath [24], and finally they were placed in a Cu cellulose coated grille. Surface acid amount and type of samples were obtained by Fourier transform infrared spectroscopy of pyridine adsorption (Py-IR) on a Thermo Nicolet NEXUS IR spectrometer equipped with a MCT detector.

The sampling of the sulfided catalysts was performed in a glove box under Ar atmosphere to avoid their partial reoxidation. The samples were crushed and pressed onto the sample holder via a double side carbon tape. Then the sample holder was moved directly to the introduction chamber of the XPS spectrometer. The X-ray photoelectron spectroscopy (XPS) analysis were performed with a PHI Quanta SXM™ spectrometer equipped with a hemispherical analyzer operating at a fixed pass energy of 40 eV and working under vacuum (<10⁻⁹ mbar). The spectra were excited by the unmonochromatised Al Kα radiation (1486.6 eV) run at 14 kV and 15 mA, and the binding energies (BE) were corrected by referencing all the energies to the C 1 s set at 284.5 eV. The Co 2p spectra were analyzed with the software Apollo Series 3500, applying a Shirley background subtraction and Gaussian-Lorentzian decomposition parameters with 20/80 Gaussian/Lorentzian proportion. The BE values were estimated to be accurate within ±0.2 eV and the methodology used for the decomposition of the spectra is explained below.

2.3. Catalytic performance tests

2.3.1. Effect of impregnation sequence on the catalytic performance

The catalytic performance of bimetallic CoMo catalysts with different impregnation sequence in selective HDS of FCC gasoline was evaluated in a high pressure fixed-bed continuous flow micro-reactor under the following conditions: reaction temperature of 250 °C, hydrogen partial pressure of 2 MPa, volume space velocity of 4 h⁻¹, hydrogen/feed volumetric ratio of 300/1 and catalyst loading of 5 ml (4.0 g). The hydrocarbon compositions of the reactant feeds and products were analyzed using a PONA-GC (Agilent 7890N). The total sulfur content was determined by Analytikjena's elemental analysis (Multi EA 3100). Finally, according to [23], the HDS activ-

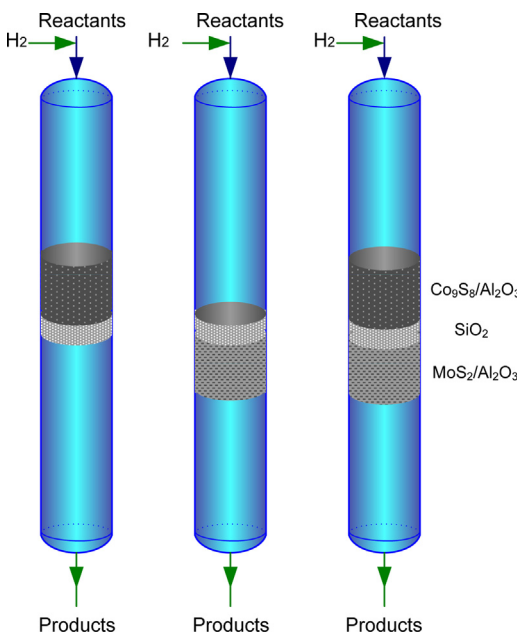


Fig. 1. Stack models of monometallic catalysts.

ity (HDS%), HYD activity of olefins (HYD%) and HDS selectivity factor (S) of the catalysts were calculated.

2.3.2. Effect of hydrogen spillover on the catalytic performance

The synergistic effects between the $\text{Co}_9\text{S}_8/\gamma\text{-Al}_2\text{O}_3$ and $\text{MoS}_2/\gamma\text{-Al}_2\text{O}_3$ catalyst on the HDS of S-compounds using 1 wt.% 2-methyl thiophene (2MT) in toluene as a model feedstocks, and on the hydrogenation of olefins using 10 wt% cyclohexene in toluene as a model feedstocks, were studied by the layered loading of model catalyst, respectively. The stack models were shown in Fig. 1. A sample of 4 g of $\text{Co}_9\text{S}_8/\gamma\text{-Al}_2\text{O}_3$ or $\text{MoS}_2/\gamma\text{-Al}_2\text{O}_3$ catalyst was used for constituting the corresponding individual bed. The arrangement of stacked beds, named as $\text{Co}_9\text{S}_8/\text//\text{MoS}_2$, were made as follows: following the reactant flow direction, the first bed was constituted by 4 g $\text{Co}_9\text{S}_8/\gamma\text{-Al}_2\text{O}_3$ catalyst and the second bed by 4 g $\text{MoS}_2/\gamma\text{-Al}_2\text{O}_3$ catalyst, the two beds were separated by 1 g SiO_2 particles. The remaining space in the reactor was filled with SiO_2 particles. The reaction conditions were as follows: reaction temperature of 200~250 °C, hydrogen partial pressure of 2 MPa, volume space velocity of 4 h⁻¹, hydrogen/feed volumetric ratio of 300/1. After a stabilizing period of 6 h, the reaction product samples were hourly collected, and analyzed using an Agilent 6820 gas chromatograph equipped with a flame ionization detector (FID) and a HP-5 capillary column (30 m × 0.32 mm × 0.5 μm). In order to measure the synergistic effect in HDS of 2MT, A synergism factor, $SF_S = \text{HDS}_{\text{Co}/\text//\text{Mo}}/(\text{HDS}_{\text{Co}} + \text{HDS}_{\text{MoS}_2})$, was defined, where HDS_{Co} and $\text{HDS}_{\text{MoS}_2}$ are the 2MT HDS conversions in single beds, and $\text{HDS}_{\text{Co}/\text//\text{Mo}}$ is the HDS conversion in composite bed system. According to the SFs, a synergism factor, $SF_0 = \text{HYD}_{\text{Co}/\text//\text{Mo}}/(\text{HYD}_{\text{Co}} + \text{HYD}_{\text{MoS}_2})$, was defined to measure the synergistic effect in olefin saturation, where HYD_{Co} and $\text{HYD}_{\text{MoS}_2}$ are the olefin saturation conversions in single beds, and $\text{HYD}_{\text{Co}/\text//\text{Mo}}$ is the olefin saturation conversion in composite bed system.

3. Results and discussion

3.1. Characterization of catalysts

3.1.1. XRD

Fig. 2 shows the XRD patterns of the sulfurized catalysts and $\gamma\text{-Al}_2\text{O}_3$. It could be seen that the $\text{Co}_9\text{S}_8 + \text{MoS}_2/\gamma\text{-Al}_2\text{O}_3$ cata-

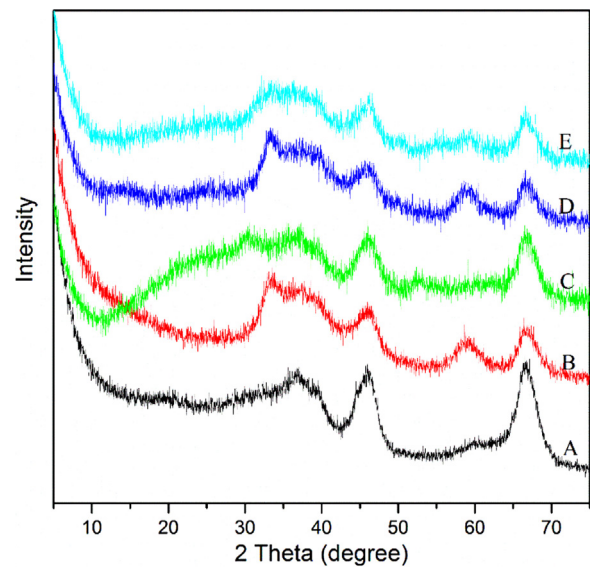


Fig. 2. XRD patterns of the sulfurized catalysts. (A) $\gamma\text{-Al}_2\text{O}_3$, (B) $\text{MoS}_2/\gamma\text{-Al}_2\text{O}_3$, (C) $\text{Co}_9\text{S}_8/\gamma\text{-Al}_2\text{O}_3$, (D) $\text{Co}_9\text{S}_8 + \text{MoS}_2/\gamma\text{-Al}_2\text{O}_3$, (E) $\text{MoS}_2 + \text{Co}_9\text{S}_8/\gamma\text{-Al}_2\text{O}_3$.

lyst prepared with first loading of Co had similar diffraction peaks with the $\text{MoS}_2/\gamma\text{-Al}_2\text{O}_3$ catalyst, presenting the diffraction peaks of 101 and 110 at $2\theta = 33.1^\circ$ and 58.5° , characteristic of MoS_2 , respectively, indicating that the first supported cobalt after sulfidation might slightly affect the morphology and structure of the latter supported MoS_2 crystallites. However, for the $\text{MoS}_2 + \text{Co}_9\text{S}_8/\gamma\text{-Al}_2\text{O}_3$ catalyst, the intensity of peaks (101) and (110) significantly weakened, implying that the latter addition of Co might decorate the edges and corners of the MoS_2 crystallites, thus forming the $(\text{Co})\text{MoS}_2$ phase and decreasing the diffraction peak intensity of MoS_2 . This results also indicated that for the $\text{Co}_9\text{S}_8 + \text{MoS}_2/\gamma\text{-Al}_2\text{O}_3$ catalyst, the Co species after sulfidation would probably form the Co_9S_8 phase, and the interaction between the sulfurized Co and MoS_2 phases was weak, and thus that the Co species would have a greater probability of forming the Co_9S_8 phase. Therefore, the step impregnation sequence of Co and Mo species could affect the interactions between Co and MoS_2 phases and thus influence the construction of the final active phase.

3.1.2. TPR

Fig. 3 represents the TPR profiles of the sulfurized catalysts. It could be seen that the $\text{MoS}_2/\gamma\text{-Al}_2\text{O}_3$ catalyst presented a strong TPR peak at 285 °C and a broad peak at 524 °C. Obviously, the high-temperature reduction peak above 400 °C attributed to the partial reduction of the small MoS_2 crystalline [25], low-temperature reduction peak at 285 °C attributed to the easily reducible sulfur on the surface of MoS_2 crystalline [26,27]. Compared to the $\text{MoS}_2/\gamma\text{-Al}_2\text{O}_3$ catalysts, the addition of Co strongly drove the shift of the both peak positions of the $\text{MoS}_2 + \text{Co}_9\text{S}_8/\gamma\text{-Al}_2\text{O}_3$ catalyst to ~221 °C and ~380 °C, respectively, indicated that the great synergism effect between Co and Mo could optimize the electrical structure of the Mo sulfide and thereby weaken the strength of Mo-S [25], and thus enhanced the reducibility of Mo sulfide. However, for the $\text{Co}_9\text{S}_8 + \text{MoS}_2/\gamma\text{-Al}_2\text{O}_3$ catalyst, the low-temperature reduction peak shifted to the 234 °C, which was higher than that of the $\text{MoS}_2 + \text{Co}_9\text{S}_8/\gamma\text{-Al}_2\text{O}_3$ catalyst, and the high-temperature reduction peak only slightly decreased to 486 °C and the area was almost the same as the $\text{MoS}_2/\gamma\text{-Al}_2\text{O}_3$ catalyst. In addition, the Co_9S_8 phase reduction peak at 615 °C could also be seen on the $\text{Co}_9\text{S}_8 + \text{MoS}_2/\gamma\text{-Al}_2\text{O}_3$ catalyst, indicated that the interaction between Co and Mo species was greatly weakened and the Co_9S_8 phase was exist on the $\text{Co}_9\text{S}_8 + \text{MoS}_2/\gamma\text{-Al}_2\text{O}_3$ catalyst. Therefore, it was reasonably con-

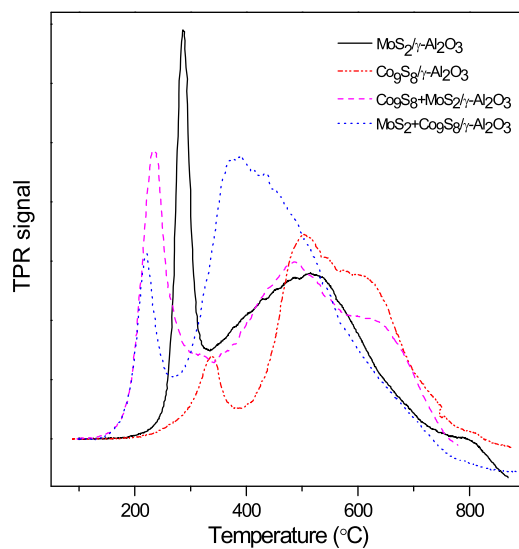


Fig. 3. TPR profiles of the sulfurized catalysts.

cluded that for the $\text{MoS}_2 + \text{Co}_9\text{S}_8/\gamma\text{-Al}_2\text{O}_3$ catalyst, the Co species added in the second step of the impregnation, could be better dispersed at the edges and corners of MoS_2 crystallites, and significantly reduced the temperature of the reduction peak. However, for the $\text{Co}_9\text{S}_8 + \text{MoS}_2/\gamma\text{-Al}_2\text{O}_3$ catalyst, Co species added in the first step of the impregnation would have a greater probability to form the Co_9S_8 phase, and the interaction between the sulfurized Co and MoS_2 phases was weak. The formed Co_9S_8 phase could generate the active hydrogen, weakening the intensity of Mo-S bridges and decreasing the temperature of the low-temperature reduction peak but slightly affected the high-temperature reduction peak. These findings also suggested that the addition sequence of Co and Mo species could affect the final structure of the active phase.

3.1.3. HRTEM

Representative HRTEM images of the sulfurized $\text{CoMo}/\gamma\text{-Al}_2\text{O}_3$ catalysts prepared by different impregnation-sulfurization sequences are given in Fig. 4. Well-stacked MoS_2 slab-like structures were regularly distributed on the surface of the support, and the distance of any two adjacent labs (0.61 nm) was the typical crystal plane spacing of MoS_2 [28]. Compared to the $\text{MoS}_2 + \text{Co}_9\text{S}_8/\gamma\text{-Al}_2\text{O}_3$ catalyst, the Co_9S_8 crystallites with the crystal plane spacing of 0.20 nm could also be seen on the surface of the $\text{Co}_9\text{S}_8 + \text{MoS}_2/\gamma\text{-Al}_2\text{O}_3$ catalyst, suggesting that the first loading Co species after sulfidation would probably form the Co_9S_8 phase, and the interaction between the sulfurized Co and MoS_2 phases was weak, and thus likely exist with two irrelevant phases, which was in agreement with the results of XRD and TPR analysis.

3.1.4. XRD of the non-supported catalysts

Fig. 5 shows the XRD patterns of the unsupported CoMo catalysts after sulfurization. The unsupported Co_9S_8 catalyst prepared from $\text{Co}(\text{NO}_3)_2 \cdot 6\text{H}_2\text{O}$ by sulfiding in a mixture of 10% vol. H_2S in H_2 presented the characteristic peaks of Co_9S_8 . It could be also seen that the unsupported MoS_2 - Co_9S_8 catalyst presented weak CoS_2 peaks and no Co_9S_8 peaks, indicated that in the MoS_2 - Co_9S_8 catalyst preparation process, the latter supported cobalt nitrate would be evenly distributed on the surface of MoS_2 phase, which could promote the interaction between Co and MoS_2 phases, thus most likely forming the $\text{Co}-\text{MoS}_2$ phase. However, for the unsupported Co_9S_8 - MoS_2 catalyst and the mechanical mixing Co_9S_8 - MoS_2 catalyst, both showed identical MoS_2 and Co_9S_8 diffraction peaks, most like the simple superposition of the peaks belonging to the unsupported Co_9S_8

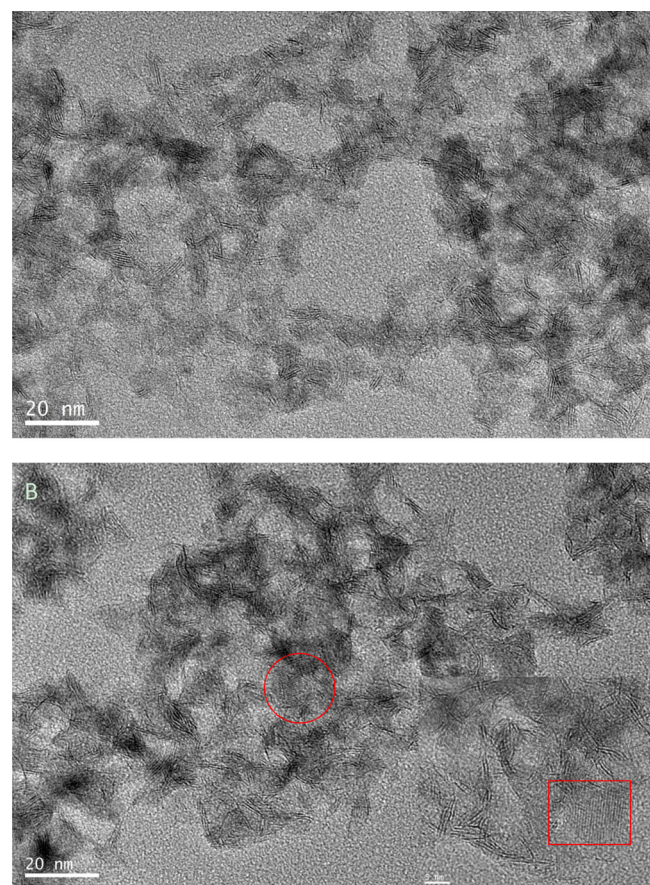


Fig. 4. HRTEM images of the sulfurized $\text{CoMo}/\gamma\text{-Al}_2\text{O}_3$ catalysts obtained with different impregnation-sulfurization sequences. (A) $\text{MoS}_2 + \text{Co}_9\text{S}_8/\gamma\text{-Al}_2\text{O}_3$, (B) $\text{Co}_9\text{S}_8 + \text{MoS}_2/\gamma\text{-Al}_2\text{O}_3$.

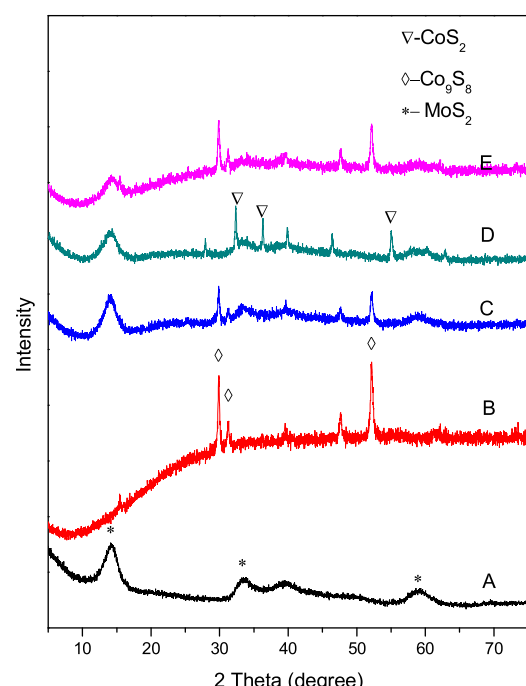
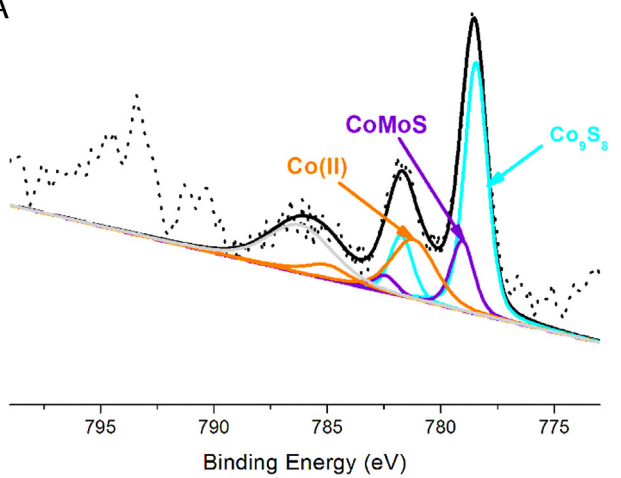


Fig. 5. XRD patterns of the non-supported catalysts. (A) MoS_2 , (B) Co_9S_8 , (C) $\text{Co}_9\text{S}_8-\text{MoS}_2$, (D) $\text{MoS}_2-\text{Co}_9\text{S}_8$, (E) $\text{Co}_9\text{S}_8/\text{MoS}_2$.

A



B

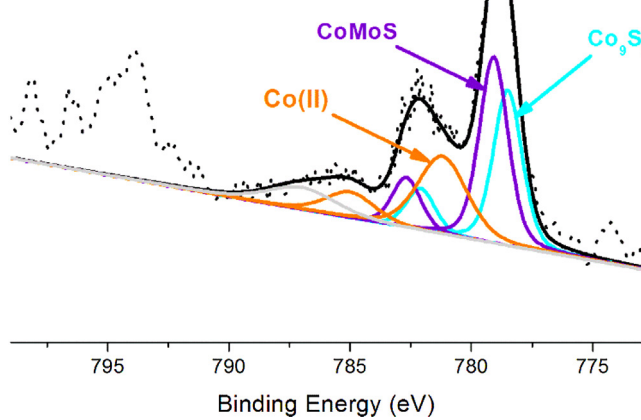


Fig. 6. Co 2p XPS spectra of the sulfurized $\text{CoMo}/\gamma\text{-Al}_2\text{O}_3$ catalysts with different impregnation-sulfurization sequences. (A) $\text{Co}_9\text{S}_8 + \text{MoS}_2/\gamma\text{-Al}_2\text{O}_3$, (B) $\text{MoS}_2 + \text{Co}_9\text{S}_8/\gamma\text{-Al}_2\text{O}_3$.

catalyst and MoS_2 catalyst. This results indicated that the interaction between Co_9S_8 and MoS_2 phases was weak, and formed Co_9S_8 phase would slightly affect the structure of the MoS_2 phase. This could better explain that more Co_9S_8 phases were formed on the surface of the supported $\text{Co}_9\text{S}_8 + \text{MoS}_2/\gamma\text{-Al}_2\text{O}_3$ catalyst prepared with first loading of Co.

3.1.5. XPS

Fig. 6 presents the experimental and fitted XPS spectra of the Co 2p for the $\text{CoMo}/\gamma\text{-Al}_2\text{O}_3$ catalysts with different impregnation sequences. According to Ref. [29] and [30], after sulfidation, the Co species was exhibited as surface cobalt oxide Co(II), CoMoS phase, and sulfided Co_9S_8 . The Co 2p_{3/2} signal centered at 781.5 eV was attributed to cobalt oxide Co(II). The Co 2p binding energy of CoMoS phase was located at 778.6 eV, while the signal for Co_9S_8 was found at 778.1 eV, even if the position difference between the two sulfided Co species was only 0.5 eV, which was the limit of resolution in the experimental conditions [30,31]. The decomposition results of the Co 2p spectra of the catalysts with different impregnation sequences are shown in Table 1. The Co_9S_8 phase represented 58.8% of the total Co on the $\text{Co}_9\text{S}_8 + \text{MoS}_2/\gamma\text{-Al}_2\text{O}_3$ catalyst was higher, on the contrary, the CoMoS phase only represented 14.7% was lower, than that of the $\text{MoS}_2 + \text{Co}_9\text{S}_8/\gamma\text{-Al}_2\text{O}_3$ catalyst. It could be ascribed

Table 1

XPS parameters of the different contributions Co 2p obtained for the sulfurized $\text{CoMo}/\gamma\text{-Al}_2\text{O}_3$ catalysts with different impregnation-sulfurization sequences.

Catalyst	Co_9S_8		CoMoS		Co (II)	
	BE (eV)	%At	BE (eV)	%At	BE (eV)	%At
$\text{Co}_9\text{S}_8 + \text{MoS}_2/\gamma\text{-Al}_2\text{O}_3$	778.1	58.8	778.6	14.7	781.3	26.5
$\text{MoS}_2 + \text{Co}_9\text{S}_8/\gamma\text{-Al}_2\text{O}_3$	778.2	33.0	778.7	40.9	781.5	26.1

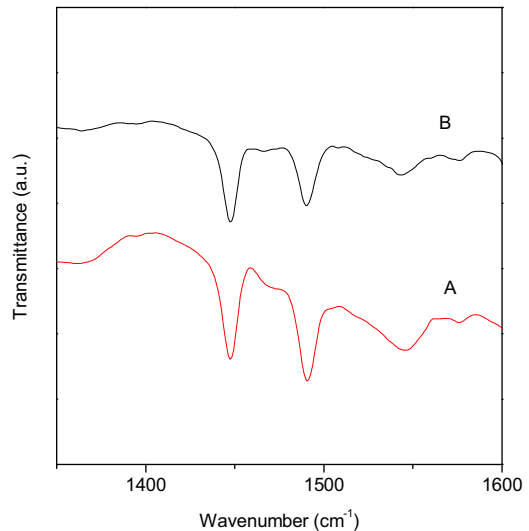


Fig. 7. FT-IR spectra of pyridine adsorbed on the sulfurized $\text{CoMo}/\gamma\text{-Al}_2\text{O}_3$ catalysts with different impregnation-sulfurization sequences. (A) $\text{Co}_9\text{S}_8 + \text{MoS}_2/\gamma\text{-Al}_2\text{O}_3$, (B) $\text{MoS}_2 + \text{Co}_9\text{S}_8/\gamma\text{-Al}_2\text{O}_3$.

to that the $\text{Co}_9\text{S}_8 + \text{MoS}_2/\gamma\text{-Al}_2\text{O}_3$ catalyst with first loading of Co would have a greater probability of forming Co_9S_8 phase, thus lead to the lower Co decoration of the MoS_2 to form the mixed CoMoS phase.

3.1.6. Py-IR

Fig. 7 shows the FT-IR spectra of pyridine adsorbed on the sulfidized catalysts to probe the acidity of the catalysts. It could be seen that three bands appeared in the spectrum of the samples at 1450 cm^{-1} , 1490 cm^{-1} and 1540 cm^{-1} . The band at 1450 cm^{-1} due to pyridine bound to the Lewis acid sites, corresponded to coordination on the Al^{3+} Lewis acid sites or the coordinatively unsaturated sites (CUS) on the MoS_2 phase of the catalysts; the band at 1540 cm^{-1} was characteristic of pyridine adsorption on the Brønsted acid sites, corresponded to the coordination on the SH groups of the MoS_2 phase of the catalysts; the band at 1490 cm^{-1} can be assigned to pyridine co-adsorbed on both Lewis and Brønsted acid sites [32]. However, the Lewis band area included the contribution of the support, which has been almost constant irrespective of the severity of the treatment [33], and the support showed no Brønsted acidity. Therefore, the observed variation of the acidic band area could be only attributed to the changes of the sulfide phase induced by the different impregnation sequence.

As shown in Fig. 7, for the $\text{Co}_9\text{S}_8 + \text{MoS}_2/\gamma\text{-Al}_2\text{O}_3$ catalyst, the Lewis band intensity was slight higher than that of the $\text{MoS}_2 + \text{Co}_9\text{S}_8/\gamma\text{-Al}_2\text{O}_3$ catalyst, however, the Brønsted band intensity was significant higher, thus showing higher B/L ratio, implied that the MoS_2 phase over the catalyst with first loading of Co formed more SH group and CUS than those of the catalyst with second loading of Co. It might be ascribed to the more Co_9S_8 phase formed on the $\text{Co}_9\text{S}_8 + \text{MoS}_2/\gamma\text{-Al}_2\text{O}_3$ catalyst, which could generate more spillover hydrogen acting on the easily reducible sulfur on the sur-

face of MoS₂ crystalline to form more active sites, namely more CUS and SH group.

From Figs. 2 and 5, the first supported cobalt after sulfidation, probably formed the Co₉S₈ phase, would slightly affect the morphology of the latter supported MoS₂ crystallites, thus showing almost the similar diffraction peaks as the MoS₂ phase. The TPR analysis results also showed that the high-temperature reduction peak of the Co₉S₈ + MoS₂/γ-Al₂O₃ catalyst only slightly decreased and the area was almost the same as the MoS₂/γ-Al₂O₃ catalyst, while the isolated Co₉S₈ phase reduction peak was also appeared, which was visibly confirmed by the HRTEM analysis. Moreover, the XPS results showed that the Co₉S₈ phase content of the total Co on the Co₉S₈ + MoS₂/γ-Al₂O₃ catalyst was 58.8%, which was extremely higher than 33% of the MoS₂ + Co₉S₈/γ-Al₂O₃ catalyst. Therefore, the interaction between the sulfurized Co and MoS₂ phases over the Co₉S₈ + MoS₂/γ-Al₂O₃ catalyst with first loading of Co was weak, and thus the Co species would have a greater probability to form the Co₉S₈ phase, leading to the extremely decreased Co decoration on the MoS₂ phase to form the CoMoS phase. This result could be explained by the catalyst preparation process. During the preparation of the MoS₂ + Co₉S₈/γ-Al₂O₃ catalyst, Co species could selectively occupy the edges and corners of MoS₂ phase to form the Co-Mo-S phase, however, during the preparation of the Co₉S₈ + MoS₂/γ-Al₂O₃ catalyst, the Co species was firstly sulfurized to the Co₉S₈ phase at 10 vol.% H₂S/H₂ atmosphere in the first step, which would be difficult to redistribute on the MoS₂ phase, leading to the lower Co decoration on the MoS₂ phase to form the mixed CoMoS phase, thus forming more Co₉S₈ phase. It was reasonably concluded that the step impregnation-sulfurization sequence of Co and Mo species could modify the interaction between the sulfurized Co and MoS₂ phases, and thus affected the final morphology and composition of the metal sulfide active phase.

In addition, the step impregnation-sulfurization sequence could also affect the number and type of active sites. From Fig. 3, the peak area of the low-temperature reduction of the Co₉S₈ + MoS₂/γ-Al₂O₃ catalyst was larger than that of the MoS₂ + Co₉S₈/γ-Al₂O₃ catalyst, while the low-temperature reduction peak originated from the easily reducible sulfur atoms on the catalyst surface, was widely accepted to measure the total number of active sites. These meant that the catalyst prepared with first loading Co had more active sites, which was also confirmed by the higher Lewis and Brønsted band intensity in Fig. 7, namely the more CUS sites and SH groups. It could be ascribed to that the more Co₉S₈ phase formed on the Co₉S₈ + MoS₂/γ-Al₂O₃ catalyst could generate more spillover hydrogen acting on the easily reducible sulfur on the surface of MoS₂ crystalline to form more active sites. The CUS sites and SH groups were considered to be two types of active sites, while the former was responsible for the hydrogenation and the latter was for the direct desulfurization [34–38]. So, the step impregnation-sulfurization sequence of Co and Mo species could affect the selectivity and activity in HDS of FCC gasoline.

3.2. Catalytic performance evaluation

3.2.1. Effect of impregnation sequence on the catalytic performance

The catalytic performance of the catalysts prepared by different step impregnation-sulfurization in terms of selective HDS of FCC gasoline is presented in Table 2. The catalyst selectivity factor S, defined to compare the selectivity of different catalysts conveniently, was calculated as a ratio of the pseudo-first-order reaction rate constants for the HDS of total sulfur and the HYD of olefins. The catalyst with larger S value presented higher selectivity. Apparently, compared to the MoS₂ + Co₉S₈/γ-Al₂O₃ catalyst, the Co₉S₈ + MoS₂/γ-Al₂O₃ catalyst showed higher HDS activity, higher olefin saturation activity and higher selectivity (S). Based on the

Table 2

Effect of impregnation sequence on the catalytic performance of the CoMo/γ-Al₂O₃ catalysts.

Catalyst	HYD(%)	HDS(%)	S
MoS ₂ + Co ₉ S ₈ /γ-Al ₂ O ₃	11.6	80.2	13.1
Co ₉ S ₈ + MoS ₂ /γ-Al ₂ O ₃	12.1	85.5	15.0

Table 3

Effect of hydrogen spillover on the HDS of 2MT.

Catalyst Bed	HDS (%)			
	200 °C	210 °C	220 °C	230 °C
Co ₉ S ₈ /γ-Al ₂ O ₃	0	0	0	0
MoS ₂ /γ-Al ₂ O ₃	2.45	3.64	5.86	8.64
Co ₉ S ₈ //MoS ₂	19.24	21.57	24.94	28.79
SF _S	7.9	5.9	4.3	3.3

Table 4

Effect of hydrogen spillover on the hydrogenation of cyclohexene.

Catalyst Bed	HYD (%)			
	200 °C	210 °C	220 °C	230 °C
Co ₉ S ₈ /γ-Al ₂ O ₃	1.80	1.74	1.75	1.79
MoS ₂ /γ-Al ₂ O ₃	13.83	13.98	15.89	21.56
Co ₉ S ₈ //MoS ₂	15.80	16.22	18.49	25.28
SF _O	1.01	1.03	1.05	1.08

characterization results above, more Co₉S₈ phases were found on the surface of the catalyst prepared with first loading of Co, which could promote the formation of Hso proposed by the remote control model [3–5]. The Hso could migrate to the MoS₂ phase and create active sites to catalyze either HDS or HYD reactions [13,39]. Therefore, it was reasonably concluded that the higher activity and selectivity of the Co₉S₈ + MoS₂/γ-Al₂O₃ catalyst would be related to the more Hso formation on the Co₉S₈ phase.

3.2.2. Effect of Hso on the catalytic performance

The synergistic effects between the Co₉S₈/γ-Al₂O₃ and MoS₂/γ-Al₂O₃ catalyst on the HDS of S-compounds and on the hydrogenation of olefins were further studied by the layered loading of model catalyst, respectively. The stack models were shown in Fig. 1.

3.2.2.1. Effect of Hso on 2MT HDS reaction. Table 3 shows the HDS conversion of 2MT over the single Co₉S₈/γ-Al₂O₃ and MoS₂/γ-Al₂O₃ beds, as well as the stacked bed Co₉S₈//MoS₂ at different temperatures. The Co₉S₈/γ-Al₂O₃ catalyst was inactive in HDS of 2MT under these conditions, but the HDS activity of the MoS₂/γ-Al₂O₃ catalyst increased with the increasing temperatures.

In the stacked-bed system, the HDS activity of the Co₉S₈//MoS₂ catalysts monotonously increased as the increasing temperatures, which was in agreement with the MoS₂/γ-Al₂O₃ catalyst. A very conspicuous result was that, the HDS conversion values of the stacked bed were significantly higher than the conversion sum of the Co₉S₈/γ-Al₂O₃ and MoS₂/γ-Al₂O₃ catalysts at all temperatures. The reaction conditions were same in all tests, and the Co-Mo-S phase could not occur due to 1 g SiO₂ particles used to separate two beds. The HDS synergism was expressed by synergism factor (SFs) defined as the ratio of the HDS conversion of the stacked bed to the conversion sum of the two signal beds. From Table 3, it could be seen that the SFs decreased with the temperature increasing. The results proved the existence of synergistic effect between the Co₉S₈/γ-Al₂O₃ and MoS₂/γ-Al₂O₃ catalysts through Hso.

3.2.2.2. Effect of Hso on olefin saturation reaction. Table 4 shows the hydrogenation conversion of cyclohexene over the single

$\text{Co}_9\text{S}_8/\gamma\text{-Al}_2\text{O}_3$ and $\text{MoS}_2/\gamma\text{-Al}_2\text{O}_3$ beds, as well as the stacked bed $\text{Co}_9\text{S}_8/\text{MoS}_2$ at different temperatures. The conversion values of the $\text{Co}_9\text{S}_8/\gamma\text{-Al}_2\text{O}_3$ catalyst were about 1.7% at all temperatures. The conversion values of the $\text{MoS}_2/\gamma\text{-Al}_2\text{O}_3$ catalyst were higher than those of the $\text{Co}_9\text{S}_8/\gamma\text{-Al}_2\text{O}_3$ catalyst and the olefin saturation activity increased with the increasing temperatures.

In the stacked-bed system, the olefin saturation activity of the $\text{Co}_9\text{S}_8/\text{MoS}_2$ catalysts also increased with the increasing temperatures. A very conspicuous result was that the HYD conversion values for the stacked bed were almost the same as the conversion sum of the single $\text{Co}_9\text{S}_8/\gamma\text{-Al}_2\text{O}_3$ and $\text{MoS}_2/\gamma\text{-Al}_2\text{O}_3$ catalysts at all temperatures. The reaction conditions concerning catalysts, loading and evaluation were same in all tests, and the Co-Mo-S phase could not occur due to 1 g SiO_2 particles used to separate two beds. Similarly, the HYD synergism was expressed by synergism factor (SFo). It could be seen in Table 4, the SFo with values in the range of 1.01 ~ 1.08 increased slightly with the temperature increasing. It could be concluded that the synergism between the Co_9S_8 and MoS_2 phases, namely the Hso, had very little effect on the olefin hydrogenation. To our knowledge, this is the first time to propose the synergism effect law of Hso in olefin saturation with the $\text{Co}_9\text{S}_8/\text{MoS}_2$ catalyst system.

Comparing the SFs and SFo in Tables 3 and 4, the results showed that the synergistic effect (Hso) significantly improved the HDS activity of the S-compounds 3–8 times, however showed slightly effect on the saturation of olefins. The remote control model [3–5] pointed out that the Hso formed on the Co_9S_8 phase by the dissociation of H_2 due to its metallic activity, could quickly spill over onto the surface of the MoS_2 and CoMoS phase to increase the CUS concentrations. The CUS sites could easily adsorb the sulfides, thus greatly improving the HDS activity. Therefore, the catalysts prepared with the first impregnation-sulfurization of Co showed higher HDS activity.

Moreover, the sulfur mobility on the catalytic active phase was dependent on the bond strength of the metal sulfide. The Mo-S bond decorated by the Co ions was the weakest and followed by that for non-decorated S-edge and Mo-edge [40,41]. Therefore, the Hso acting as electron donors and showing stronger reductive would completely remove the sulfur at the Co-Mo-S edge and at the S-edge to form the multi-CUS sites, and partially remove the sulfur at the Mo-edge to form the SH sites. Based on the XPS analysis, more Co_9S_8 phase were formed on the $\text{Co}_9\text{S}_8 + \text{MoS}_2/\gamma\text{-Al}_2\text{O}_3$ catalyst compared to the $\text{MoS}_2 + \text{Co}_9\text{S}_8/\gamma\text{-Al}_2\text{O}_3$ catalyst. This meant that more Hso would be formed in the $\text{Co}_9\text{S}_8 + \text{MoS}_2/\gamma\text{-Al}_2\text{O}_3$ catalyst, which could act on the (Co)MoS₂ phase to create more multi-CUS sites and more SH sites, which was proved by the FT-IR results. It was widely accepted that the multi-CUS site was responsible for the indirect desulfurization route and the SH site was for the direct desulfurization route [34–38]. Therefore, the $\text{Co}_9\text{S}_8 + \text{MoS}_2/\gamma\text{-Al}_2\text{O}_3$ catalyst showed higher HDS activity.

The very little effect of Hso on the olefin saturation could be explained by that the Hso showing strong reduction ability could easily transfer to the surface of MoS_2 phase, and create a large number of multi-CUS as active sites for indirect desulfurization, while the created number of the low CUS sites ascribed to active sites for olefin saturation was relatively less [42,43]. Therefore, the synergistic effect could significantly improve the HDS activity, but showed very little effect on the olefin saturation.

According to the above analysis, the step impregnation-sulfurization sequence of Co and Mo species could modify the interaction between the sulfurized Co and MoS_2 phases. The Co species was sulfurized to the Co_9S_8 phase in the first step, which would be difficult to redistribute on the MoS_2 phase, leading to the lower Co decoration on the MoS_2 phase to form the mixed CoMoS phase, thus forming more Co_9S_8 phase. The more formed Co_9S_8 phase could not only performed as a support to improve the

distribution of the MoS_2 phase but also produce the Hso by dissociation of H_2 , to create a large number of multi-CUS and SH groups, but less low CUS sites, thus greatly improved the HDS activity and selectivity and showed very little effect on the olefin saturation.

4. Conclusions

In this report, the promoter Co synergism effect on the performance of MoS_2 phase in selective HDS of FCC gasoline was studied by regulating the step impregnation-sulfurization sequence of Co and Mo to adjust the formation probability of Co-Mo-S phase and the separated Co_9S_8 and MoS_2 phases. The evaluation results demonstrated that the catalyst with Co species first impregnation and followed sulfurization showed higher HDS activity and selectivity. According to the data obtained by XRD, HRTEM, XPS, TPR and FT-IR analysis, the interaction between the sulfurized Co and MoS_2 phases over the $\text{Co}_9\text{S}_8 + \text{MoS}_2/\gamma\text{-Al}_2\text{O}_3$ catalyst with Co first loading was weak, and the sulfurized Co species would be difficult to redistribute on the MoS_2 phase, leading to the lower Co decoration on the MoS_2 phase to form the mixed CoMoS phase, thus forming more Co_9S_8 phase. The more formed Co_9S_8 phase could produce more Hso to create a large number of CUS and SH groups, thus greatly improving the HDS activity and selectivity. The Hso effect between the Co_9S_8 and MoS_2 phases in HDS of 2MT, especially on olefin hydrogenation was originally studied by using a single bed and stacked beds catalyst system. It was found that the Hso could significantly improve the HDS activity, but showed very little effect on HYD of olefins.

Acknowledgements

This work was supported by grants from the Major State Basic Research Development Program of China (973 Program, 2010CB226905) and the Fundamental Research Funds for the Central Universities (Grants No.14CX06112A, No.15CX07002A and No.15CX02023A)

References

- [1] C. Song, Catal. Today 86 (2003) 211–263.
- [2] G. Berhault, M.P. De la Rosa, A. Mehta, M.J. Yacaman, R.R. Chianelli, Appl. Catal. A 345 (2008) 80–88.
- [3] J.M. Asua, B. Delmon, Appl. Catal. 12 (1984) 249–262.
- [4] L. Portela, P. Grange, B. Delmon, J. Catal. 156 (1995) 243–254.
- [5] B. Delmon, G.F. Froment, Cat. Rev. Sci. Eng. 38 (1996) 69–100.
- [6] H. Topsøe, B.S. Clausen, N.-Y. Topsøe, P. Zeuthen, Stud. Surf. Sci. Catal. 53 (1989) 77–102.
- [7] H. Topsøe, B.S. Clausen, R. Candia, C. Wivel, S. Mørup, J. Catal. 68 (1981) 433–452.
- [8] C. Wivel, R. Candia, B.S. Clausen, S. Mørup, H. Topsøe, J. Catal. 68 (1981) 453–463.
- [9] N.-Y. Topsøe, H. Topsøe, J. Catal. 84 (1983) 386–401.
- [10] C. Geantet, M. Vrinat, Appl. Catal. A 322 (2007) 1–2.
- [11] J. Ojeda, N. Escalona, P. Baeza, M. Escudéy, F.J. Gil-Llambias, Chem. Commun. (2003) 1608–1609.
- [12] K. Inamura, R. Prins, J. Catal. 147 (1994) 515–524.
- [13] P. Baeza, M.S. Ureña-Zanartu, N. Escalona, J. Ojeda, F.J. Gil-Llambias, B. Delmon, Appl. Catal. A 274 (2004) 303–309.
- [14] P. Baeza, M. Villarroel, P. Avila, A.L. Agudo, B. Delmon, F.J. Gil-Llambias, Appl. Catal. A 304 (2006) 109–115.
- [15] M. Villarroel, P. Baeza, N. Escalona, J. Ojeda, B. Delmon, F.J. Gil-Llambias, Appl. Catal. A 345 (2008) 152–157.
- [16] M. Villarroel, P. Baeza, F. Gracia, N. Escalona, P. Avila, F.J. Gil-Llambias, Appl. Catal. A 364 (2009) 75–79.
- [17] N. Escalona, R. García, G. Lagos, C. Navarrete, P. Baeza, F.J. Gil-Llambias, Catal. Commun. 7 (2006) 1053–1056.
- [18] R. Prins, Chem. Rev. 112 (2012) 2714–2738.
- [19] C. Navarrete, R. García, C. Sepulveda, F.J. Gil-Llambias, J.L.G. Fierro, N. Escalona, Catal. Lett. 141 (2011) 1796–1802.
- [20] M. Villarroel, E. Camu, N. Escalona, P. Avila, S.B. Rasmussen, P. Baeza, F. Gil-Llambias, Appl. Catal. A (2011) 63–68.
- [21] M. Egorova, R. Prins, J. Catal. 225 (2004) 417–427.
- [22] T.G. Kaufmann, A. Kaldor, G.F. Stuntz, M.C. Kerby, L.L. Ansell, Catal. Today 62 (2000) 77–90.

- [23] B. Liu, Y. Chai, Y. Li, A. Wang, Y. Liu, C. Liu, *Appl. Catal. A* 471 (2014) 70–79.
- [24] Y.P. Li, A.T. Li, F.F. Li, D.P. Liu, Y.M. Chai, C.G. Liu, *J. Catal.* 317 (2014) 240–252.
- [25] B. Yoosuk, J.H. Kim, C. Song, C. Ngamcharussrivichai, P. Prasassarakich, *Catal. Today* 130 (2008) 14–23.
- [26] P. Afanasiiev, *Appl. Catal. A* 303 (2006) 110–115.
- [27] C.H. Jacobsen, E. Törnqvist, H. Topsøe, *Catal. Lett.* 63 (1999) 179–183.
- [28] R. Nava, J. Morales, G. Alonso, C. Ornelas, B. Pawelec, J.L.G. Fierro, *Appl. Catal. A* 321 (2007) 58–70.
- [29] A.D. Gandubert, E. Krebs, C. Legens, D. Costa, D. Guillaume, P. Raybaud, *Catal. Today* 130 (2008) 149–159.
- [30] M. Ramos, G. Berhault, D.A. Ferrer, B. Torres, R.R. Chianelli, *Catal. Sci. Technol.* 2 (2012) 164–178.
- [31] I. Alstrup, I. Chorkendorff, R. Candia, *J. Catal.* 77 (1982) 397–409.
- [32] T. Mochizuki, H. Itou, M. Toba, Y. Miki, Y. Yoshimura, *Energy Fuel* 22 (2008) 1456–1462.
- [33] G. Berhault, M. Lacroix, M. Breysse, F. Maugé, J.-C. Lavalle, H. Nie, L. Qu, *J. Catal.* 178 (1998) 555–565.
- [34] S.H. Yang, C.N. Satterfield, *Ind. Eng. Chem. Prod. Res. Dev.* 23 (1984) 20–25.
- [35] M. Jian, R. Prins, *Catal. Today* 30 (1996) 127–134.
- [36] T.C. Ho, *Catal. Rev. Sci. Eng.* 30 (1988) 117–160.
- [37] B. Liu, Y.M. Chai, Y.P. Li, A.J. Wang, Y.Q. Liu, C.G. Liu, *Fuel* 123 (2014) 43–51.
- [38] B. Liu, Y.M. Chai, Y.P. Li, A.J. Wang, Y.Q. Liu, C.G. Liu, *Appl. Catal. A* 471 (2014) 70–79.
- [39] Y.W. Li, B. Delmon, *J. Mol. Catal. A* 127 (1997) 163–190.
- [40] A. Ishihara, F. Dumeignil, D.H. Wang, X.G. Li, H. Arakawa, E.W. Qian, S. Inoue, A. Muto, T. Kabe, *J. Jpn. Pet. Inst.* 48 (2005) 37–44.
- [41] F. Dumeignil, J.F. Paul, E. Veilly, E.W. Qian, A. Ishihara, E. Payen, T. Kabe, *Appl. Catal. A* 289 (2005) 51–58.
- [42] S. Hatanaka, M. Yamada, *Ind. Eng. Chem. Res.* 36 (1997) 1519–1523.
- [43] S. Hatanaka, M. Yamada, *Ind. Eng. Chem. Res.* 36 (1997) 5110–5117.